International Journal of GEOMATE, Feb., 2025 Vol.28, Issue 126, pp.1-7
ISSN: 2186-2982 (P), 2186-2990 (O), Japan, DOI: https://doi.org/10.21660/2025.126.4713
Geotechnique, Construction Materials and Environment

# DETERIORATION OF REINFORCED CONCRETE STRUCTURES DUE TO CHLORIDE EXPOSURE IN WATER: A CASE STUDY, THAILAND

*Mallika Nguanthaisong[1], Bantita Terakulsatit[2], Watcharakon Setwong[3], and Chalermluck Phoovasawat[4]

[1, 2] School of Geotechnology, Institute of Engineering, Suranaree University of Technology, Thailand.
[3, 4] Synchrotron Light Research Institute (SLRI), Nakhon Ratchasima, Thailand

*Corresponding Author, Received: 09 Sep. 2024, Revised: 06 Nov. 2024, Accepted: 14 Nov. 2024

**ABSTRACT:** Saline soils in Northeast Thailand, particularly in Nakhon Ratchasima Province, pose a significant threat to the durability of reinforced concrete structures. Chloride infiltration from these soils accelerates steel corrosion, reducing the service life of concrete. This study investigates chloride penetration in concrete within saline environments and examines the oxidation states of iron under varying chloride levels. Using X-ray Absorption Spectroscopy (XAS), changes in iron phases were analyzed before and after brine exposure. Concrete samples were immersed in chloride solutions to simulate local conditions in Nakhon Ratchasima, aiming to calculate the chloride diffusion coefficient and predict concrete deterioration. The findings will help in selecting suitable cement types to enhance durability in saline conditions and guide efforts to mitigate reinforced concrete corrosion in the region. The study also examines chloride penetration in reinforced concrete immersed in chloride solutions for 30, 60, and 90 days at various chloride concentrations. Chloride levels were measured at depths of 2, 4, and 6 cm from the concrete surface, in accordance with ASTM C1152 standards. Results indicate the highest chloride concentration near the surface, decreasing with depth, with prolonged exposure increasing chloride infiltration. XAS analysis of deformed bar samples identified iron oxides such as FeO(OH) and $Fe_2O_3$, which are integral to the corrosion process. The study highlights that a 30% increase in chloride concentration above the actual maximum measured in a saline environment significantly accelerates steel-reinforced concrete corrosion, substantially impacting the durability and lifespan of these structures.

*Keywords: Chloride content, XAS, XANES, Reinforced concrete, Deformed bars.*

## 1. INTRODUCTION

The largest saline soil area in Thailand is located in Nakhon Ratchasima Province, encompassing approximately 2.5 million rai [1]. This region faces significant issues related to both saline soil and water. Non Thai District in Nakhon Ratchasima Province, is situated in a region characterized by extensive salt-bearing geological formations, particularly the Maha Sarakham Formation. This formation contributes to the high salinity levels in groundwater and water, including elevated concentrations of chloride ions. Natural processes, such as the dissolution of salts from underground formations, are compounded by human activities, including irrigation, urbanization, and industrial discharge, which exacerbate chloride contamination in water resources [2].

The presence of chloride in saline water has far-reaching implications for various sectors, such as agriculture, water supply, and infrastructure development. In Non Thai District, the elevated chloride content in water poses not only a threat to water quality but also significant challenges for the durability of concrete structures. Prolonged exposure to chloride-laden saline water can lead to the deterioration of concrete, compromising the safety and longevity of infrastructure. In general, chloride-induced corrosion of steel reinforcement in concrete can cause cracking, spalling, and even structural failure, raising both economic and safety concerns [3]. The corrosion process involves redox reactions leading to the formation of FeO and various corrosion layers composed of Fe(II), Fe(III), and mixed Fe(II)/Fe(III) compounds. X-ray absorption spectroscopy (XAS) has proven effective for identifying oxidation states, particularly at the Fe K-edge, which is widely used in corrosion science [4]. X-ray absorption near-edge structure (XANES) analysis further aids in quantifying the Fe(II) to Fe(III) ratio [5], which is essential for understanding corrosion mechanisms in complex materials, such as naturally occurring iron oxides.

The findings of this research will serve as a reference for addressing corrosion in reinforced concrete structures in the saline soil regions of Nakhon Ratchasima Province. Additionally, the study aims to determine the chloride diffusion coefficient in reinforced concrete after exposure, enabling predictions of concrete deterioration. This knowledge is essential for selecting suitable cement types to enhance infrastructure durability and prevent future damage. The paper presents measurements of chloride infiltration, analysis of chloride penetration and its effects on reinforced concrete, chloride diffusion coefficient, and elemental analysis of concrete samples using X-ray Fluorescence (XRF), as well as Fe phase absorption over periods of 30, 60, and 90 days.

## 2. RESEARCH SIGNIFICANCE

Although there have been extensive studies in this area on the distribution of salinity and chloride content, along with their effects on the environment, water usage, and agriculture. There has been no study on the relationship between salinity and damage to reinforced concrete structures. This research seeks to examine the relationship between chloride presence in saline water and the deterioration of concrete structures in Non Thai District. It specifically focused on chloride penetration into concrete and analyze the oxidation states of iron under varying chloride concentrations.

## 3. MATERIALS AND METHODOLOGY

### 3.1 Materials

The cast-reinforced concrete samples have a dimension of 15x15x15 cm³. The model-reinforced concrete samples incorporate steel bars with a diameter of 12 mm and a concrete cover thickness of 5 cm (Fig. 1), made from Ordinary Portland Cement Type 1. A water-to-cement ratio of 0.45 was maintained, The curing period of 28 days was carried out by immersing the samples in water, with the containers sealed and shielded from sunlight.

Four pieces of SD40 steel bars, each 12 mm in diameter and 5 cm in length were embedded within the concrete structure during casting (Figure 1). All concrete samples were immersed in chloride solutions simulating the conditions found in Non Thai District, Nakhon Ratchasima Province, Thailand, for periods of 30, 60, and 90 days, respectively. The chloride concentrations used in the study represented the actual minimum, average, Maximum concentration [6] and Increasing 10, 20, and 30% the actual maximum concentration found in the study areas (Table 1).

Table 1. Surface water quality along Highway No. 205 in the Non Thai District, Nakhon Ratchasima Province, Thailand. Increasing 10, 20, and 30% from the actual maximum concentration found in the study areas.

| Chloride concentration level | Concentration (mg/L) |
|---|---|
| Minimum concentration (Min) | 1186.44 |
| Average concentration (Avg) | 2004.37 |
| Maximum concentration (Max) | 4548.02 |
| Increasing 10% of Max | 5028.20 |
| Increasing 20% of Max | 5457.62 |
| Increasing 30% of Max | 5912.43 |

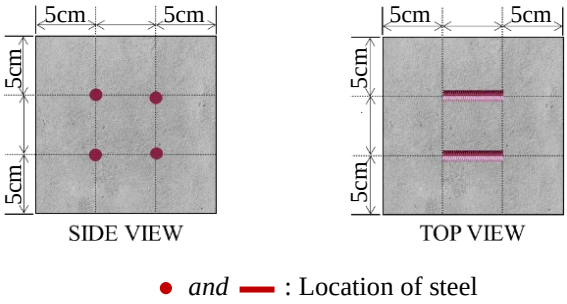


Fig 1. The cross-section of cube concrete.

### 3.2 Immersion Principle for Concrete Structure

*3.2.1 Chloride infiltration measurement*

(1) Collect chloride powder samples from three concrete cube layers (approximately 2, 4, and 6 cm from the surface). Grind the samples until each layer weighs about 50 g.

(2) Determine the chloride content using the ASTM C1152 titration method to analyze total chloride penetration The experiment to determine was conducted three times, and the results were subsequently used to calculate the chloride diffusion rate. Estimate chloride diffusion coefficients at each time interval using Fick's 2nd Law [7], based on the measured chloride levels from the three layers. The variations in chloride penetration measurements are influenced by the specific types of cement and the water-to-cement ratio used.

(3) The effect of concrete cover distance (C) on these measurements is less understood, it can be a significant parameter in structural design for evaluating structural deterioration. $D_{ap}$ represents the penetration of chloride into concrete, which affects the durability of structures.

$$C_{cl}(t,x) = C_0 - \mathrm{erf}\frac{x}{2\sqrt{D_{ap}\cdot t}} \quad (1)$$

where $C_{cl}$ (t, X)is the chloride content at any time and location in concrete.

$C_0$ is chloride concentration on the concrete surface (at X=0) at water soaking time t

$D_{ap}$ is the penetration of chloride into concrete or chloride penetration coefficient)

T is the duration

X is the depth of a concrete surface

erf is an error function.

*3.2.2 Chloride penetration and its effects on reinforced concrete analysis.*

To study chloride penetration in reinforced concrete, a model of the study area's salinity environment will be created. X-ray Absorption Spectroscopy (XAS) will be used to examine iron

before and after exposure to various brine concentrations. The study includes two sample types: corrosion powder from deformed bars and cross-section concrete samples cured for 28 days (C28). Six of 10 mg powder samples were prepared and measured in transmission mode, while the cross-section samples were measured in fluorescence mode, as they aren't suitable for transmission mode.

The XAS experiment was performed at BL1.1W: Multipurpose X-ray Techniques (MXT) at the Synchrotron Light Research Institute (SLRI) in Nakhon Ratchasima, Thailand, using an electron energy of 1.2 GeV. The measurements focused on X-ray Absorption Near Edge Structure (XANES). Iron foil was used to calibrate the E0 of the Fe-K edge (7112 eV), and the photon energy was scanned from 150 eV below to 150 eV above this edge, with a beam size of approximately 3x4 mm. The XANES spectra were analyzed using Athena software. XAS and SEM were chosen for corrosion assessment due to their complementary capabilities. Detailed chemical information on the oxidation states and environments of elements involved in corrosion was provided by XAS, while high-resolution surface imaging and structural analysis were offered by SEM. Together, they allowed for a comprehensive evaluation of both the chemical and physical aspects of corrosion, making them ideal tools for a thorough understanding of the corrosion process.they allowed for a comprehensive evaluation of both the chemical and physical aspects of corrosion, making them ideal tools for a thorough understanding of the corrosion process.

## 4. RESULTS AND DISCUSSION

### 4.1 Chloride Penetration

Chloride levels were measured from reinforced concrete immersed in chloride solutions for 30, 60, and 90 days, with concentration levels at 10%, 20%, and 30% of the maximum concentration. Concrete powders were collected at depth levels of 2, 4, and 6 cm from the concrete surface. The amount of infiltrated chloride in the reinforced concrete was measured according to the ASTM C1152 standard for total chloride content. This study compares the total chloride penetration in reinforced concrete at different depth levels and immersion durations of 30, 60, and 90 days.

The experiment illustrates that chloride penetration into reinforced concrete decreases with increasing depth from the concrete surface. The highest concentration of chloride is observed within the depth range of 0-2 cm, with concentrations progressively decreasing at greater depths, as depicted in Table 2 and Fig. 2. However, measurable chloride levels at greater depths exceed those at shallower depths. Such occurrences may arise in porous reinforced concrete structures, influenced by factors such as variations during the cement casting process. Fig. 2 illustrate scenarios where the porous structure contributes to higher cumulative chloride concentrations.

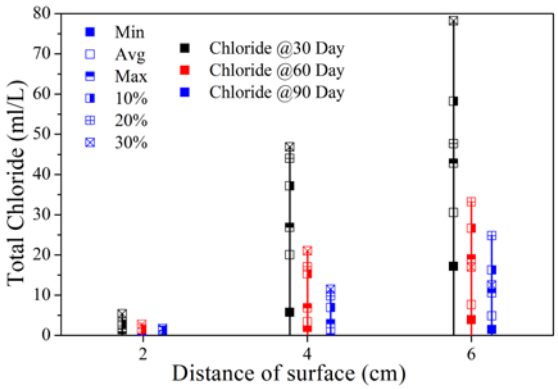


Fig 2. Total chloride concentration (ml/L) at various surface distances (cm) after immersion in a chloride solution. The highest chloride content was detected in samples soaked for 90 days at surface distances up to 2 cm, while the lowest chloride content was observed in samples soaked for 30 days at depths of 4-6 cm.

Table 2. Effect of total chloride content (TCC) on reinforced concrete immersed in a chloride solution for 30, 60, and 90 days at different surface distances. (Standard Deviation < 0.2%)

| Chloride | Surface distance (cm) | 30 days TCC (ml/L) | 60 days TCC (ml/L) | 90 days TCC (ml/L) |
|---|---|---|---|---|
| Min | 0-2 | 1.34 | 5.61 | 17.00 |
| | 2-4 | 0.48 | 1.91 | 3.90 |
| | 4-6 | 0.48 | 1.05 | 1.34 |
| Avg | 0-2 | 1.91 | 19.85 | 30.38 |
| | 2-4 | 1.91 | 3.33 | 7.60 |
| | 4-6 | 1.05 | 1.34 | 4.76 |
| Max | 0-2 | 2.48 | 26.68 | 42.63 |
| | 2-4 | 1.05 | 6.75 | 18.99 |
| | 4-6 | 0.48 | 2.76 | 10.45 |
| 10% of Max | 0-2 | 2.76 | 36.93 | 58.01 |
| | 2-4 | 1.05 | 15.29 | 26.68 |
| | 4-6 | 0.48 | 6.75 | 16.15 |
| 20% of Max | 0-2 | 3.33 | 43.77 | 47.47 |
| | 2-4 | 1.91 | 17.00 | 33.23 |
| | 4-6 | 1.05 | 9.60 | 24.69 |
| 30% of Max | 0-2 | 5.33 | 46.62 | 77.94 |
| | 2-4 | 2.76 | 20.99 | 17.00 |
| | 4-6 | 0.48 | 11.31 | 12.44 |

Fig. 3 (A) and (B) Study the physical properties of concrete using an SEM (Scanning Electron Microscope) to investigate the microstructure formation of cement when exposed to chloride content, illustrates that the interior of the concrete exhibits voids and numerous perforations predominantly caused by chloride corrosion, ultimately affecting the crystalline structure of the concrete. This situation can persist with prolonged exposure to chloride, highlighting the critical role of reinforced concrete longevity in managing cumulative chloride concentrations, particularly in

environments with high chloride levels. This suggests a potential for ongoing infiltration until the internal chloride concentration aligns with that of the external environment. In concrete structures, there exist voids and numerous perforations, shaping the distinct crystalline texture predominantly composed of calcium aluminate oxide, carbonate hydrate (C-A), and calcium silicate oxide (C-A-O). These voids harbor elongated, needle-like crystals reminiscent of ettringite mineral formations, originating from the swift reaction between tricalcium aluminate and water, subsequently forming hydrated calcium aluminate in conjunction with gypsum [8].

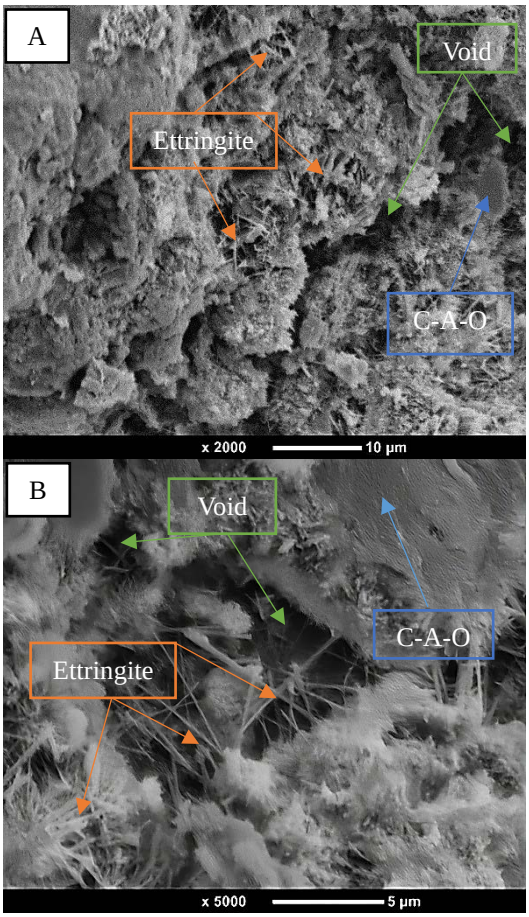


Note: refer to ettringite
refer to C-A-O
refer to void

Fig 3. Scanning Electron Microscope (SEM) of concreate. Ettringite is formed from the hydration reaction, while the porosity of cement can generally be categorized into two types: gel pores and capillary pores. (A) 2,000x magnification and (B) 5,000x magnification.

### 4.2 Coefficient of Chloride Diffusion

Chloride penetrates concrete structures through mechanisms such as diffusion, permeation, and capillary action. When the concrete structure becomes saturated without pressurization from water, chloride diffusion becomes the primary mechanism. This implies that chloride penetration is influenced by concentration differentials, determining the direction of infiltration from areas of higher to lower chloride concentration, following Fick's 2nd Law of Diffusion.

The ASTM C1152 standard titration method is specifically designed to measure chloride diffusion at different depths, focusing on determining the total chloride content in concrete. This approach allows for the calculation of the chloride penetration coefficient (Dap) and surface chloride concentration (Cs), following Fick's 2nd Law of Diffusion, using real chloride diffusion data as reference points.By evaluating exposure times of 30, 60, and 90 days and comparing them with the estimated Dap over the same periods, it becomes evident that this coefficient depends significantly on exposure duration. Longer exposure times result in lower $D_{ap}$ values due to enhanced hydration reactions and increased strength of the concrete structure (Fig. 4).

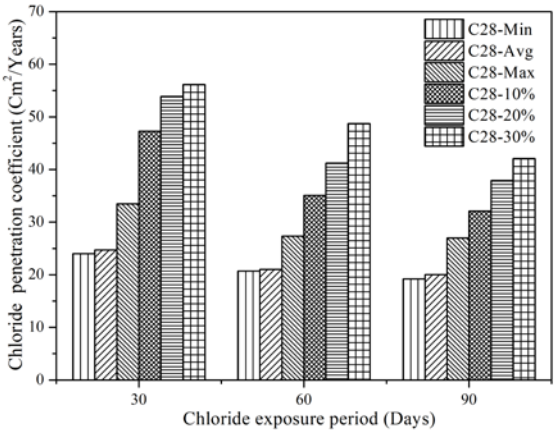


Fig 4. The chloride penetration coefficient ($cm^2$/year) with chloride exposure period (days). The chloride diffusion coefficient of concrete was found to vary based on the duration of chloride exposure. It was observed that as the exposure time increased, the chloride diffusion coefficient of the concrete decreased

### 4.3 Elemental Analysis of Concrete Samples using X-ray Fluorescence (XRF)

The study involved analyzing the type and quantity of trace elements in concrete sample powder, which was cured for 28 days and then soaked in solutions with varying chloride concentrations: the lowest, highest, and average concentrations, as well as concentrations, increased by 10, 20, and 30% from the highest concentration. The immersion times were 30, 60, and 90 days. Analysis revealed that prolonged exposure to chloride led to a gradual decrease in the fundamental constituents of the concrete at various depths (Fig. 5). This decline was due to the infiltration of chloride ions, which caused significant corrosion, particularly at the concrete surface. Consequently, the

ratio of primary concrete elements decreased, while the ratio of chloride ions increased with extended exposure. The chloride ion content consistently rose during the immersion periods but diminished gradually with increasing distance from the concrete surface.

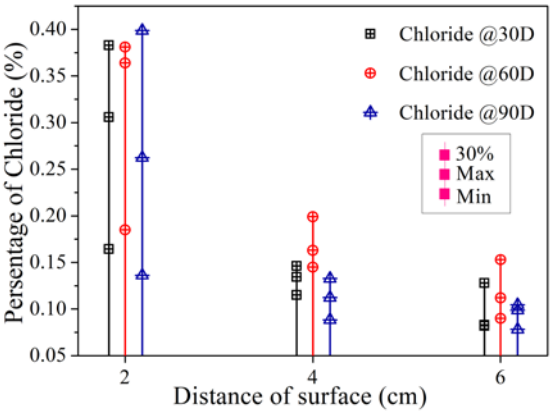


Fig 5. Percentages of chloride were analyzed using X-ray fluorescence (XRF). The chloride content detected decreased with both the immersion duration and the distance from the surface of the concrete sample.

### 4.4 Fe Phase Absorption

The XANES feature comparison of the Fe-K edge absorption utilized Fe-foil and Fe ion standards, including Fe-foil metals for E0 calibrations, as well as FeO, $Fe_2O_3$, FeO(OH), and $FeCl_2 \cdot 4H_2O$. Since the powder and cross-section deformed bar samples were measured in different absorption modes, the Fe standards were measured in both modes for analysis.

The examination of concrete-immersed deformed bar samples revealed varying extents of alteration across different areas. Specifically, the rusted surface (Red face) exhibited more pronounced changes in the Fe phase compared to the side surface (Side face), which showed minimal effects in the hand specimen. The cross-section white face represents the original deformed bar material from the industry. The XANES spectra of Fe standards are compared with the XANES spectra of the three regions of the deformed bar in fluorescence mode (Fig. 6).

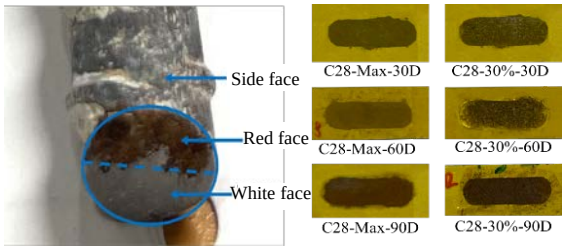


(a) (b)

Fig 6. The sample of deformed bar using to XAS as (a) Deformed bar and (b) Powders

The XANES feature of deformed bars are found to mirror those of Fe materlic (Fe foil) but exhibit a tendency to shift to higher energies due to oxidation processes, progressing sequentially through the white, side, and red faces. The white face of the deformed bar, primarily composed of iron carbide ($Fe_3C$), is observed to show a leftward shift in XANES relative to Fe foil standards, attributed to the sample's greater thickness during measurement, which results in higher fluorescent signal and self-absorption effects.

A shift towards higher absorption energy with an increased white line peak is exhibited by the side face of the deformed bar, attributed to immersion in chloride solution and subsequent Fe oxidation. The red face XANES feature is characterized by a significant mix of Fe oxides within the metallic Fe, marked by the highest white line peak and a shift to higher absorption energy. Consistent indications of Fe material oxidation due to immersion in chloride solution are provided by the derivative XANES features, with a notable decrease in Fe foil intensity at 7112 eV and a significant change in the red face derivative features between 7118-7130 eV, reflecting iron oxide characteristics [9]. Changes in the Fe phase post-immersion in chloride solution are revealed by the cross-sectional XANES features of the deformed bar, though the specific Fe oxide phases remain uncharacterized. X-ray synchrotron fluorescence mode analysis is applied to penetrate both the bulk volume and surface of the deformed bar, resulting in XANES features that average all incident X-rays showed in Fig. 7.

Additionally, powdered samples collected solely from the deformed bar's surface under various concrete immersion conditions in chloride solution are utilized in this study to characterize the iron oxide phase. The powder sample exhibited the highest chloride concentration in Non-Thai water, surpassing the maximum chloride concentration by 30%. Two distinct chloride concentrations were tested over immersion periods of 30, 60, and 90 days. The powder samples were prepared in sample holders sealed with Kapton tape, and the iron phases were analyzed using XAS techniques at BL1.1W-SLRI, focusing on the XANES Fe-K edge (7112 eV).

The XANES spectra of the powder samples were compared with those of Fe ion standards, including Fe-foil, FeO, $Fe_2O_3$, FeO(OH), and $FeCl_2 \cdot 4H_2O$, under the same transmission mode XAS measurement. The various Fe standard phases exhibited distinct XANES features, marked by the symbols a, b, c, d, and e, indicating their respective peak positions and characteristics.

The powder samples predominantly contained $Fe^{3+}$, as evidenced by the absorption edge and the position of the first derivative feature between 7124-7127 eV. The XANES features of both chloride concentrations and immersion durations exhibited a

trend consistent with a mixture of three Fe standards: $Fe_2O_3$, FeO(OH), and $FeCl_2{\cdot}4H_2O$. However, the mixing ratios varied with the duration of immersion. Analysis of the 1st derivative feature, as shown in Fig 8, indicated that samples immersed for 30 days had the highest $Fe_2O_3$ content, while the $FeCl_2{\cdot}4H_2O$ mixing ratio increased after 60 days. By 90 days, the FeO(OH) compound became predominant. Linear combination fitting (LCF) software was employed to evaluate the Fe standard mixing ratios, using a fitting range 20 eV below and above the 7112 eV 1st derivative feature of the powder samples. The fitting results, shown in Table 3. revealed a decreasing trend in $Fe_2O_3$ and an increasing trend in FeO(OH) across both chloride concentration levels for immersion periods of 30, 60, and 90 days.

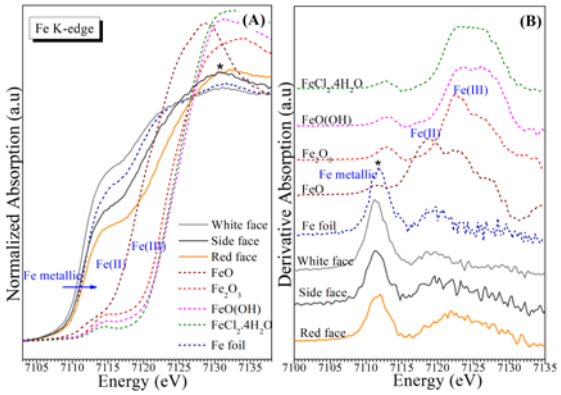


Fig 7. The XANES spectrum of the cross-section of the deformed bar is compared to the Fe foil and Fe oxide standards as (a) normalized and (b) 1st derivative.

This experiment suggests that with a 30% higher chloride concentration in Non-Thai water, initial deformed bars in concrete are susceptible to chloride water penetration. After 30 days, high FeO(OH) levels indicate that Fe particles on the deformed bar surface react more readily with oxygen from the water. At 60 days, the Fe reaction results in increased $Fe_2O_3$, possibly indicating the formation of a passive film before significant corrosion occurs [10]. By 90 days, the Fe phase transitions predominantly to FeO(OH) due to the accumulation of $Cl^-$ ions in the chloride water, which destroys the passive film and accelerates deformed bar corrosion [11], resulting in high FeO(OH) levels.

For the maximum chloride concentration in Non-Thai water, similar Fe phase mixing and reactions occur at 30 and 60 days as observed with the 30% concentration. However, after 90 days, the chloride ion concentration is insufficient to completely destroy the passive film and cause extensive corrosion, leading to the continued presence of $Fe_2O_3$ alongside FeO(OH). The observed Fe phases from the deformed bar can explain the differing effects of chloride concentration on the degradation of the deformed bar, with the $Fe_2O_3$ component of the passive film providing some protection against corrosion at 90 days under maximum chloride conditions (Fig. 9).

Table 3. The Fe standard mixing ratio by using linear combination fitting (LCF).

| Samples | Chi-square | R-factor |
|---|---|---|
| C28-30%-30D | 0.00569 | 0.0174054 |
| C28-30%-60D | 0.00186 | 0.0042864 |
| C28-30%-90D | 0.0084 | 0.0167673 |
| C28-Max-30D | 0.00317 | 0.0070804 |
| C28-Max-60D | 0.00282 | 0.0063954 |
| C28-Max-90D | 0.00099 | 0.0017903 |

| Samples | Standard | | |
|---|---|---|---|
| | FeO(OH) | $FeCl_2.4H_2O$ | $Fe_2O_3$ |
| C28-30%-30D | 0.554 (0.025) | 0.192 (0.016) | 0.254 (0.037) |
| C28-30%-60D | 0.464 (0.026) | 0.098 (0.007) | 0.438 (0.035) |
| C28-30%-90D | 0.829 (0.010) | 0.171 (0.010) | - |
| C28-Max-30D | 0.625 (0.023) | 0.163 (0.014) | 0.212 (0.035) |
| C28-Max-60D | 0.391 (0.033) | 0.114 (0.014) | 0.495 (0.042) |
| C28-Max-90D | 0.580 (0.019) | 0.079 (0.006) | 0.341 (0.030) |

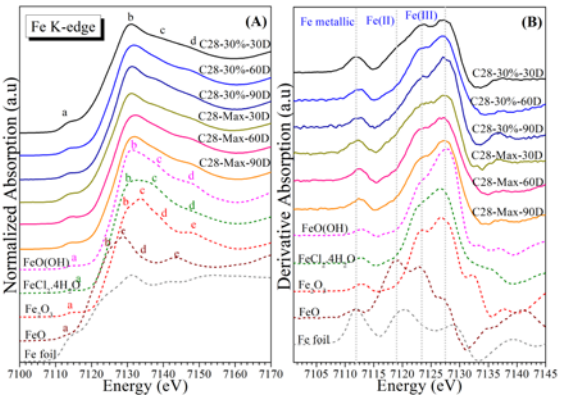


Fig 8. XANES Fe K-edge of powder samples were comparison the Fe standard including, Fe-foil, FeO, $Fe_2O_3$, FeO(OH), and $FeCl_2{\cdot}4H_2O$ as (a) normalized and (b) 1st derivative.

## 5. CONCLUSIONS

The depth of chloride penetration in concrete exposed to chloride solutions of varying concentrations over periods of 30, 60, and 90 days significantly affects the reinforced steel structure. Chloride levels are highest at the surface, diminishing

with distance from the surface, and increasing with longer exposure durations. Structural fractures lead to the formation of voids in the concrete, which, in turn, elevate chloride concentrations. Therefore, monitoring chloride levels within the reinforced structure is essential for detecting structural damage. The chloride penetration coefficient (Dap) decreases with prolonged exposure, suggesting that ongoing hydration enhances the density and organization of the concrete structure.

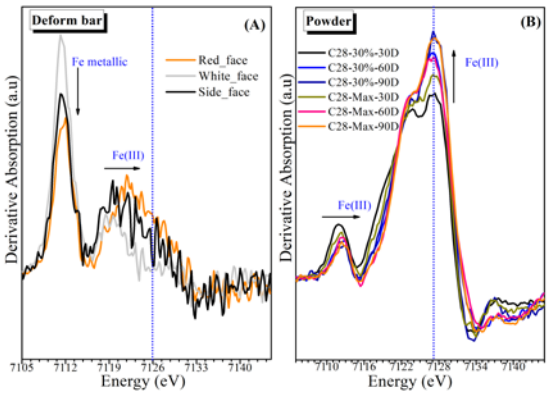


Fig 9. XANES Fe K-edge of powder samples and deform bars were analyzed in 1st derivative absorption intensities.

Analyzing the iron phases in deformed bar samples using XANES proved challenging, but powder samples offered insights into the iron phases present under various chloride concentrations and exposure times. X-ray penetration in bulk deformed bar samples, analyzed through the 1st derivative, indicated a trend of increasing iron oxide and decreasing metallic iron. XANES analysis of powder samples highlighted corrosion involving $Fe^{3+}$ species, influenced by FeO(OH) and $Fe_2O_3$ phases, which play a crucial role in protecting the deformed bar from corrosion. However, comparing the spectra of powder samples with iron standards identified alterations and phases like $Fe_3O_2$, FeO(OH), and $FeCl_2{\cdot}4H_2O$. Ultimately, in this study, chloride concentrations exceeding 30% in Non-Thai water were found to contribute significantly to the corrosion of deformed bars over 90 days, indicating that chloride has a profound impact on the corrosion process. To extend the lifespan of reinforced concrete structures, selecting a concrete type that is resistant to chloride induced corrosion, along with considering the previously mentioned factors, is essential.

## 6. ACKNOWLEDGMENTS

This work was financially supported by (i) Suranaree University of Technology (SUT), (ii) Thailand Science Research and Innovation (TSRI), and (iii) National Science, Research and Innovation Fund (NSRF) under the grant numbers: NRIIS 179329. Special Thank you to BL1.1 Section: Multiplies X-ray Techniques, Synchrotron Light Research Institute (SLRI), Nakhon Ratchasima, Thailand.

## 7. REFERENCES

[1] Jackhapun P., Salinity Management in Nakhon Ratchasima. Land Development Department, Thailand, 2016, pp. 1-116.

[2] Phoemphon W. and Terakulsatit B., Assessment Of Groundwater Potential Zones and Mapping Using GIS/RS Techniques and Analytic Hierarchy Process: A Case Study on Saline Soil Area, Nakhon Ratchasima, Thailand. AIMS Geosciences 2022, 2022, pp. 49-67.

[3] Stephen John C., Bernardo A. and Jason Maximino C., Corrosion Behavior Analysis of Self-Compacting Concrete Using Impressed Current and Rapid Chloride Penetration Test, International Journal of GEOMATE, Vol.24, Issue 101, 2023, pp.76-83.

[4] Cornell R and Schwertmann U., The Iron Oxides: Structure, Properties, Reactions, Occurrences and Uses (New York: Wiley), 2013, pp. 1-664.

[5] Wilke M, Farges F, Petit P-E, Brown G E and Martin F., Oxidation State and Coordination of Fe in Minerals: a FeKXANES Spectroscopic Study, Am. Mineral 86 714-30, 2001, pp. 714-730.

[6] Terakulsatit B., Glumglomjit S., Hanta R., Phuphlub T. and Nguanthaisong M., Assessment of Surface Water Quality Distribution to Identify Risky Areas of Reinforced Concrete Structure Deterioration: A Case Study along Saranarai Road (Highway No. 205), Non Thai District, Nakhon Ratchasima, Thailand. 2023, Proceedings of Iasteminternational Conference Singapore, 2023, pp. 13-19.

[7] Jens M. F., Leif M. and Lars N., Fick's 2nd - Complete Solutions For Chloride Ingress Into Concrete, Lund Institute of Technology: Division of Building Materials, 2008, pp. 1-106.

[8] Paul E. Stutzman., Scanning Electron Microscopy in Concrete Petrography. Building and Fire Research Laboratory National Institute of Standards and Technology Gaithersburg, MD 20899 USA, 2001, pp. 59-72.

[9] Simon H., Cibin G., Freestone I. and Schofield E., Fe K-Edge X-Ray Absorption Spectroscopy of Corrosion Phases of Archaeological Iron: Results, Limitations, and The Need For Complementary Techniques. Phys. Condens. Matter 33 344002, 2021, pp. 344002-344017.

[10] Tangwei M., En-Hua Y. and Cise U., Passivation of Reinforcing Steel in Reactive Mgo Cement Blended with Portland Cement and Concrete Composites. Volume 143, October 2023, 105269, 2023, pp. 105269-105284.

[11] Tian Y., Zhang G., Hailong Y., Zeng Q., Zhang Z., Tian Z., Jin X., Jin N., Chen Z. and Wang J., Corrosion of Steel Rebar in Concrete Induced by Chloride Ions Under Natural Environments, Construction and Building Materials, 2023, pp. 130504-130529.